Isolated dSph galaxy KKs3 in the local Hubble flow

I.D. Karachentsev[1,*], **A.Yu. Kniazev**[2,3,4,**], and **M.E. Sharina**[1]

[1] Special Astrophysical Observatory, Russian Academy of Sciences, Russia
[2] South African Astronomical Observatory, PO Box 9, 7935 Observatory, Cape Town, South Africa
[3] Southern African Large Telescope Foundation, PO Box 9, 7935 Observatory, Cape Town, South Africa
[4] Sternberg Astronomical Institute, Lomonosov Moscow State University, Moscow 119991, Russia

Key words   galaxies: dwarf — galaxies: distances and redshifts

 We present the SALT spectroscopy of a globular cluster in the center of the nearby isolated dSph galaxy KKs3 situated at a distance of 2.12 Mpc. Its heliocentric radial velocity is 316 ± 7 km s^{-1} that corresponds to $V_{LG} = 112$ km s^{-1} in the Local Group (LG) reference frame. We use its distance and velocity along with the data on other 35 field galaxies in the proximity of the LG to trace the local Hubble flow. Some basic properties of the local field galaxies: their morphology, absolute magnitudes, average surface brightnesses, specific star formation rates, and hydrogen mass-to-stellar mass ratios are briefly discussed. Surprisingly, the sample of the neighboring isolated galaxies displays no signs of compression under the influence of the expanding Local Void.

1 Introduction

Numerous high-accuracy measurements of distances to nearby galaxies performed over the past 15 years with the Hubble Space Telescope showed that the regular Hubble flow starts directly outside the boundary of the Local Group (LG). As described in Karachentsev & Makarov (2001), Ekholm et al. (2001), and Karachentsev et al. (2002), the radial velocities and distances of the local field galaxies with respect to the LG centroid comply well with the Hubble relation $V_{LG} = H \times D_{LG}$. Along with this, the local value of the Hubble parameter H turns out similar to its global value, $H_0 = 73$ km s^{-1} Mpc^{-1}, and the peculiar radial velocity dispersion is only $\sigma(V_{pec}) \sim 30$ km s^{-1}. Approximately the same peculiar velocity dispersion is also typical for the barycenters of the nearby galaxy groups (Karachentsev, 2005). A considerable number of papers are devoted to the interpretation of the observed data on the "cold" Hubble flow (Chernin 2001, Chernin et al. 2004, Teerikorpi et al. 2005, Chernin 2008, Hoffman et al. 2008, Peirani & Pacheco 2008, Tikhonov & Klypin 2009, and Chernin et al. 2015).

With the low peculiar radial velocity dispersion, the curvature of the local Hubble flow, caused by the retarding gravitational influence of the LG as a local attractor, manifests itself distinctly. As reported by Karachentsev et al. (2009), the radius of the zero-velocity surface around the LG is $R_0 = (0.96 \pm 0.03)$ Mpc, to which the total mass of

the Local Group $M_T(LG) = (1.9 \pm 0.2) \times 10^{12} M_\odot$ corresponds in good agreement with the sum of individual mass estimations for the Milky Way (MW) and the Andromeda galaxy (M31).

Over the last years, the accuracy in measurements of the distances to the nearby galaxies using the tip of the red giant branch (TRGB) method was raised up to $\sim 5\%$ (Rizzi et al. 2007). The most complete reviews of the distance estimates are presented in the "Extragalactic Distance Database" (=EDD, Tully et al. 2009) and the "Updated Nearby Galaxy Catalog" (=UNGC, Karachentsev et al. 2013). Both are available at: http://edd.ifa.hawaii.edu and http://lv.sao.ru/lvgdb; the reviews are periodically updated.

It is obvious that the isolated (field) galaxies, the velocities of which are not contaminated by large virial motions such as found for group members, are the most suitable ones for tracing the local Hubble flow. When analyzing the Hubble pattern of the peculiar velocities (Karachentsev et al. 2009), 30 galaxies outside the LG with distances of 0.7 Mpc $< D_{LG} <$ 3.0 Mpc were considered. Since then, only two new dwarf galaxies, Leo P (Giovanelli et al. 2013) and KK 258 (Karachentsev et al. 2014), have been added to that list. One more isolated dSph galaxy KKs3 was recently discovered at a distance of 2.12 Mpc (Karachentsev et al. 2015), although its radial velocity was unknown. We will determine below the radial velocity for this galaxy and consider the location of KKs3 in the local Hubble flow.

2 Surface photometry of KKs3

For surface photometry, we used the fully processed distortion-corrected F606W and F814W images of KKs3 obtained with the Hubble Space Telescope Advanced Camera for Surveys (HST/ACS, SNAP 13442, PI R.B.Tully). Foreground stars were removed from the frames. The sky background in the ACS images was insignificant, but to remove possible slight large scale variations, the sky was approximated by a tilted plane created from a two-dimension polynomial with the use of the least-squares method. The accuracy of the sky background determination was about 2% of the original sky level. To measure a total galaxy magnitude in each band, a galaxy image was first fitted with concentric ellipses. Then integrated photometry was performed in these ellipses. The total magnitude was estimated as an asymptotic value of the radial growth curve. The measured total magnitude and colour turned out $V = 14.47 \pm 0.05$ and $(V - I) = 0.77 \pm 0.03$ respectively. The estimated errors include the photometry and sky background uncertainties, as well as the transformation errors from instrumental ACS magnitudes to the standard V and I magnitudes (Sirianni et al. 2005).

Azimuthally averaged surface brightness profiles for KKs3 were obtained by differentiating the galaxy growth curves with respect to semiaxes. The resulting profiles in the V and I bands are shown in Fig. 1. The surface brightness profile can be fitted by an exponential law with an exponential scale length of $34''\!.0$ and $31''\!.8$ in the V and I bands respectively. The unweighted exponential fits the profiles with an effective radius of $57''\!.0$ and $53''\!.3$ and effective surface brightness of 24.87 and 24.01 ($^m/\square''$) in the V and I bands respectively.

Observations of KKs3 with the ACS revealed a globular cluster located in the dwarf galaxy center. It produces a narrow central peak in the right upper panel of Fig. 1. Our photometry of the globular cluster yields its total magnitude $V = 18.70$ and color $V - I = 0.85$ within an aperture of $1''$ radius.

3 Spectroscopic observations of KKs3

Spectroscopic observations of the globular cluster were conducted with the Southern African Large Telescope (SALT)(Buckley et al. 2006, O'Donoghue et al. 2006) on January 15–17, 2015 with the Robert Stobie Spectrograph (RSS, Burgh et al. 2003, Kobulnicky et al. 2003). The high resolution long-slit spectroscopy mode of the RSS was used with a $1''\!.25$ slit width. The grating pg0900 with blocking filter pc03400 and Camera Station parameter 26.5 was used to cover the spectral range of 3700–6700 Å with a reciprocal dispersion of 0.97 Å pixel^{-1} and spectral resolution of FWHM=5 Å. The seeing during the observation (twilight time mostly) was about 1–2$''$. The total exposure time was 5200s divided into 5 subexposures of $\sim$1000s each in order to remove cosmic rays. A spectrum of Ne comparison

arcs was obtained to calibrate the wavelength scale. Primary reduction of the data was done with the SALT science pipeline (Crawford et al. 2010). The long-slit reduction was done later, in the way described in Kniazev et al. (2008). We note that SALT is a telescope with a variable pupil, and its illuminated beam changes continuously during the observations. This makes the absolute flux/magnitude calibration impossible, even using spectrophotometric standard stars. The one-dimensional scan of the spectrum in the range of 3700 – 6700 Å is presented in Fig. 2. As the data suggest, there are absorption Balmer lines and H and K doublet of CaII. They yield the heliocentric radial velocity $V_h = 316 \pm 7 \ \mathrm{km \ s^{-1}}$, or the Local Group centroid velocity $V_{LG} = 112 \ \mathrm{km \ s^{-1}}$.

4 The Hubble flow for the local field galaxies

The typical separation between the group centers in the Local Volume is 3–4 Mpc. Thus, we defined the local Hubble flow to have a distance limit of 3.5 Mpc. According to the UNGC catalog (Karachentsev et al. 2013), in the area of this radius there are 125 galaxies with measured radial velocities and accurate distance estimations. Each galaxy from the UNGC is characterized by a "tidal index"

$$\Theta_1 = \max[\log(M_n^*/D_n^3)] - c, \ \ n = 1, 2, \dots N,$$

where M_n^* denotes the stellar mass of the nearby galaxy and D_n is its spatial distance from the galaxy under study. Among the numerous neighbors, there is a so-called Main Disturber (=MD), the tidal force of which, $\sim M^*/D^3$, dominates all other neighbors. The parameter $c = -10.96$ was chosen so that the galaxy with $\Theta_1 < 0$ was situated outside the "zero-velocity surface" of the radius R_0 around its MD. By selecting the galaxies with a tidal index of $\Theta_1 < 0$, we excluded, thereby, all the members of the LG and of other nearby groups. As the value Θ_1 is derived with a certain error, we selected the objects with $\Theta_1 \leq 0.2$ for our sample. The fulfilment of this condition gives us a model sample of 36 field galaxies, the velocities of which do not include a considerable virial component. Table 1 shows various characteristics of these galaxies. We emphasize that the galaxies in this Table present the most complete sample of the nearby field galaxies, the properties of which suffer from observational selection effects to the minimal degree only. The characteristics of this sample can serve as a basis to check various simulations of the field galaxy population.

The observables of the galaxies from Table 1 were taken from the UNGC catalog. The table columns contain: (1) the galaxy name; (2), (3) the supergalactic coordinates; (4) the heliocentric distance of the galaxy and its error; (5) the distance of the galaxy from the LG barycenter on the assumption that it is located on the line between the MW and M31 at a distance of 0.43 Mpc away from the MW (Karachentsev et al. 2009) here; the mass ratio for two dominating galaxies, M(M31) : M(MW)=5 : 4, corresponds to that value; (6) the

heliocentric radial velocity of the galaxy and its error; (7) the radial velocity of the galaxy in the LG reference frame with the standard apex parameters adopted in the NASA Extragalactic Database (NED, http://ned.ipac.caltech.edu/); (8), (9) the tidal index Θ_1 and the name of the MD that exerts the greatest tidal force on the galaxy; (10) the peculiar radial velocity of the galaxy relative to the regression line in Fig. 3; (11) the morphological type as per de Vaucouleurs scale; (12) the average surface brightness of the galaxy in the B band within the Holmberg isophote of $26.5^m/\square''$; (13) the absolute extinction-corrected B magnitude of the galaxy; (14) the specific star formation rate which was estimated from the ultraviolet (FUV) flux measured with the GALEX satellite (Gil de Paz et al. 2007); (15) the neutral hydrogen mass-to-stellar mass ratio estimated by the luminosity of the galaxy in the K band at $M^*/L_K = 1 \times M_\odot/L_\odot$ (Bell et al. 2003). For some early-type galaxies ($T < 0$), only upper values of sSFR and M_{HI}/M^* are given.

Figure 3 shows the distribution of 36 nearest isolated galaxies by distances and radial velocities in the LG rest frame. The galaxies of late ($T > 0$) and early types are denoted by the solid and open circles respectively (with distance errors). The dashed straight line denotes the undisturbed Hubble flow with a parameter of H_0 =73 km s^{-1} Mpc^{-1}. The solid line corresponds to the regression of radial velocity on distance for a canonic Lemétre-Tolman model with the parameter $R_0 = 0.96$ Mpc.

The measured radial velocity of the dSph galaxy KKs3 fixes its position by 45 km s^{-1} lower than the regression line. The M31 galaxy exerts the greatest gravitational force on KKs3, although their mutual separation is too large for M31 to cause the high peculiar velocity of KKs3.

Apart from KKs3, the other new member of the local Hubble flow, Leo P, has a nearly zero peculiar velocity. The distance to this dwarf irregular galaxy, $D = 1.90 \pm 0.05$ Mpc, was measured by L. N. Makarova with the TRGB method using the images of this galaxy from the Hubble Space Telescope Archive (G0 13376, PI K.McQuinn).

It should be also noted that the radial velocity $V_h = -135 \pm 2$ km s^{-1} of the dSph galaxy KKR 25 at first was incorrectly estimated from the HI line (Huchtmeier et al. 2000) because of confusion with the Galactic HI line. The new estimate $V_h = -79 \pm 8$ km s^{-1} derived from the optical spectrum (Makarov et al. 2012) notably shifted the galaxy in the Hubble diagram. The same happened to the transition-type dwarf galaxy Tucana. The first estimation of its radial velocity, $V_h = -132 \pm 5$ km s^{-1}, was derived with association of the HI-cloud with it (Oosterloo et al. 1996). However, the subsequent measurements of the velocity for the galaxy stellar component increased the value by 62 km s^{-1} (Fraternali et al. 2009).

In the right upper corner of the Hubble diagram, there are five galaxies: DDO 99, DDO 125, DDO 181, UGC 8833, and DDO 190, which neighbor with each other in the sky and are situated in front of the nearby cloud of dwarf galaxies, CVnI. Attraction to the CVnI cloud may cause additional velocity directed away from the LG.

5 Peculiar velocity pattern around the LG

The apex parameters of the Sun's motion relative to the LG centroid in Galactic coordinates:

$$V_A = 316 \pm 5 \,\text{km s}^{-1}, l_A = 93° \pm 2, b_A = -4° \pm 2, (1)$$

adopted as standard in NED, were determined by velocities and distances of 20 nearest galaxies in the LG vicinity (Karachentsev & Makarov 1996). Over the last years, new galaxies have been discovered near the LG, and radial velocities and distances for a number of old ones have been refined. As a result, the parameters of the standard apex could change. Analysis of the peculiar radial velocities of nearby galaxies with respect to the standard apex (1) showed (Karachentsev et al. 2009) that there was a small dipole component with the parameters:

$$V_d = 24 \pm 4 \,\text{km s}^{-1}, l_d = 325°, b_d = -46°. \qquad (2)$$

In the supergalactic coordinates, the apex of this dipole is situated near the equator of the Local supercluster: $SGL_d = 227°, SGB_d = 1°$.

Figure 4 shows the distribution of the peculiar velocities of the nearby isolated galaxies from Table 1 depending on the supergalactic longitude. The notations for the late and early type galaxies are the same as in Fig. 3. The vertical intervals denote the errors in estimation of the galaxy velocities caused by distance errors. The wavy line corresponds to the above-mentioned dipole with an amplitude of 24 km s^{-1}. As seen from this pattern, peculiar velocities of the most galaxies follow approximately the dipole wave. Five galaxies toward the CVnI cloud (contoured), as well as Tucana and Leo A, deviate from the general tendency. Both the Tucana and Leo A are situated close to the zero-velocity surface for the LG. They might have the dynamic history different from the other, more distant LG neighbors. The peculiar velocity dispersion for all the galaxies in Fig. 4 is 32 km s^{-1}, and it decreases to 23 km s^{-1} when excluding 5 galaxies in the CVnI region. A considerable portion of this value accounts for the dipole component and the errors in distance estimation. If we take the dipole effect into consideration, the corrected values of the standard apex (1) will be as follows:

$$V_a = 314 \,\text{km s}^{-1}, l_a = 91°, b_a = -8°. \qquad (3)$$

Notice that the direction toward the closest rich cluster Virgo ($SGL = 103°, SGB = -2°$) is not associated with any characteristic feature in the pattern V_{pec} vs. SGL.

As is well-known, the LG and other neighboring galaxy groups are located within the flat structure (wall) which emborders the Local Void. Weygaert & Schaap (2007) and Tully et al. (2008) noted that a completely empty void in a topologically flat ΛCDM universe expands at a rate of 16 km s^{-1}Mpc^{-1}. If a void is not completely empty, the expansion is going at a slower rate. This fact makes us consider

the situation with local peculiar velocities depending on the supergalactic SGB latitude. Let us note that the Local Void occupies approximately one-fourth of the whole sky and its center is located close to the north supergalactic pole.

The distribution of 36 neighboring isolated galaxies by peculiar velocities and supergalactic latitude is presented in Fig. 5. The notations are the same as in the previous figure. As one can see, at high latitudes $| SGB |> 30°$ there are only 7 galaxies instead of the expected 18 with a uniform random distribution of them in the sky. Shortage in the number of galaxies in the supergalactic polar caps could be conditioned by the fact that the poles of the Local supercluster lie in the region of a considerable Galactic extinction. However, sky surveys in the HI line are almost insensitive to the extinction. For this reason, the observed shortage in gas-rich dIr galaxies in the region $| SGB |> 30°$ is probably caused by the intrinsic tendency of such kind of objects to be concentrated toward the local supercluster plane.

In the picture of the Local Void expansion, three galaxies, SagdIr, DDO 210, and KKR 25 with $SGB > +30°$ should have had negative peculiar velocities. With their average height above the supergalactic plane $\langle SGZ \rangle = +0.95 \pm 0.12$ Mpc, the expected effect for a completely empty void would have amounted to about –15 km s^{-1}. However, the observed average peculiar velocity is $(+16 \pm 11)$ km s^{-1}. Thus, we can not recognize the expected effect of the Void expansion. If the wall, in which the LG is located, moves as a whole in the direction opposite to the Local Void, then four galaxies: HIZSS3, NGC 3109, Sex A, and Sex B with $SGB < -30°$, should also have had negative peculiar velocities. Although, their position in Fig. 5 does not agree with this assumption: the average peculiar velocity of these galaxies is $+21 \pm 5$ km s^{-1}. It is obvious that the behavior of the neighboring isolated galaxies in the $\{V_{pec}, SGB\}$ diagram needs to be analyzed in detail with the involvement of reconstructing their orbits by numerical modeling (Shaya et al. 1995).

6   Some properties of the local orphan galaxies

As emphasized above, Table 1 shows the sample of the field galaxies which is least subject to various observational selection effects. It is reasonable to suppose that this sample is almost 100% luminosity complete up to the absolute magnitude $M_B = -9^m$.

Figure 6 presents a mosaic of distribution of a number of the nearest field galaxies by basic parameters: the absolute magnitude, the average surface brightness, the specific star formation rate, and the retio of neutral hydrogen mass to stellar mass of the galaxy. Five galaxies of early morphological types are highlighted in green. These data allow us to draw the following inferences.

– The main population of the field galaxies consists of dwarf galaxies with the median absolute magnitude $M_B \simeq -13.0^m$. More than half of them are gas-rich dIr galaxies (T =10) which are easily detected in the HI surveys.

– The distribution of the isolated galaxies by the average surface brightness has the peak and the median near $24.5^m/\square''$, which is typical for the members of groups and clusters. It seems unlikely that among the field dIr galaxies, there is a hidden population of objects with a very low surface brightness ($SB \geq 26^m/\square''$), which remains still undetected. However, it should be pointed out that the large population of extremely low surface brightness dSph systems (satellites of the MW and M31) was found during the last 10 years only with start of the Sloan survey and systematic studies of M31 halo. Almost all of these ultra-faint objects are dSphs. A population of such kind objects can also exist in the general field, being undetected so far with any modern HI and optical surveys.

– The field galaxy distribution by the specific star formation rate shows the peak near $\log(sSFR) \simeq -10.1$. Note that the value of sSFR is of the same dimension, yr^{-1}, as that the Hubble parameter, H_0, having the quantity $\log H_0 = -10.14$. This coincidence means that a typical representative of the field galaxies is able to reproduce its stellar mass over the cosmological time H_0^{-1} with the currently observed star formation rate.

– About 70% of the isolated galaxies are characterized by the ratio $\log(M_{HI}/M^*)$ in the range of [–0.5, +0.5] with the median –0.25. In other words, the majority of field galaxies are in the middle of their evolution process in transforming the gas component into the stellar one.

– Among the field galaxies, there are some objects of early types: KKR 25 (dSph), KKs3 (dSph), KK 258 (dTr), and Tucana (dTr), in the population of which the old stars ($t > 10^{10}$ years) prevail. These dwarf systems have low luminosity, low surface brightness, poor gas content, and low current star formation rate. To explane the presence of the isolated dSph galaxies (as well as the phenomenon of the isolated S0 galaxy NGC 404) one could invoke a scenario of "cosmic web stripping" such as proposed by Benítez-Llambay et al. (2013).

7   Concluding remarks

The studied Local Volume amounts to about 160 Mpc^3 after subtracting the "infall zones" around the LG and some other neighboring galaxy groups. In this Volume, 36 field galaxies form the average density of ~ 0.22 gg/Mpc^3. Owing to the unique proximity of the Local Volume, almost all the neighboring isolated galaxies have been detected so far. Some incompleteness of our sample can be evident in the lack of a systematic survey of the northern sky (Dec.$> +40°$) in the 21-cm line, which could supplement two–three new Leo P-type irregular dwarfs. Another reason for the data incompleteness in Table 1 can be the difficulty in detecting gas-

poor spheroidal dwarf galaxies of a low surface brightness at high supergalactic latitudes, where the optical extinction exceeds 1 mag. However, the number of the known isolated dSph galaxies in the rest of the transparent sky region is quite small.

For all the galaxies from our sample, the radial velocities are measured, and the distances are estimated with an accuracy of $\sim 5\%$. Every isolated galaxy from Table 1 has the estimations of stellar mass and mass of gas, and the data on the current star formation rate in them. The wealth and completeness of the observed data on the nearby field galaxies make this sample essential while checking various models of isolated galaxy formation by means of N-body simulations.

References

Bell, E.F., McIntosh, D.H., Katz, N., & Weinberg, M.D., 2003, ApJS, 149, 289

Benítez-Llambay A., Navarro J.F., Abadi M.G., Gottlöber S., Yepes G., Hoffman Y., Steinmetz M., 2013, ApJ, 763, L41

Buckley, D.A.H., Swart, G.P., & Meiring, J.G., 2006, in Society of Photo-Optical Instrumentation Engineers (SPIE) Conference Series Vol. 6267 of Society of Photo- Optical Instrumentation Engineers (SPIE) Conference Series, Completion and commissioning of the Southern African Large Telescope

Burgh, E. B., Nordsieck, K. H., Kobulnicky, H. A. et al., 2003, in Iye M., Moorwood A. F. M., eds, Instrument Design and Performance for Optical/Infrared Ground-based Telescopes Vol. 4841 of Society of Photo-Optical Instrumentation Engineers (SPIE) Conference Series, Prime Focus Imaging Spectrograph for the Southern African Large Telescope: optical design. p. 1463

Crawford, S. M., Still, M., Schellart, P. et al., 2010, in Society of Photo-Optical Instrumentation Engineers (SPIE) Conference Series Vol. 7737 of Society of Photo-Optical Instrumentation Engineers (SPIE) Conference Series, PySALT: the SALT science pipeline

Chernin, A.D., Emelyanov, N.V. & Karachentsev, I.D., 2015, MNRAS, 449, 2069

Chernin, A.D., 2008, UFN, 178, 267

Chernin, A.D., Karachentsev, I.D., Valtonen, M.I., et al., 2004, A&A, 415, 19

Chernin, A.D., 2001, Physics-Uspekhi, 44, 1099

Ekholm, T., Baryshev, Y., Teerikorpi, P. et al., 2001, A & A, 368, L17

Fraternali, F., Tolstoy, E., Irwin, M.J., & Cole, A.A., 2009, A & A, 499, 121

Gil de Paz, A., et al., 2007, ApJS, 173, 185

Giovanelli, R., Haynes, M.P., Adams, E.A.K., et al., 2013, AJ, 146, 15

Hoffman, Y., Martinez-Vaquero, L.A., Yepes, G., & Gottloeber, S., 2008, MNRAS, 386, 390

Huchtmeier, W.K., Karachentsev, I.D., & Karachentseva, V.E., 2000, A&A, 147, 187

Karachentsev, I.D., Makarova, L.N., Makarov, D.I., Tully, R.B., & Rizzi, L., 2015, MNRAS, 447L, 85

Karachentsev, I.D., Makarova, L.N., Tully, R. B., Wu, P.-F., & Kniazev A.Y., 2014, MNRAS, 443, 1281

Karachentsev, I.D., Makarov, D.I., & Kaisina, E.I., 2013, AJ, 145, 101 (=UNGC)

Karachentsev, I.D., Kashibadze,O.G., Makarov, D.I., & Tully, R.B., 2009, MNRAS, 393, 1265

Karachentsev, I.D., 2005, AJ, 129. 178

Karachentsev, I.D., Sharina, M.E., Makarov, D.I., et al. 2002, A&A, 389, 812

Karachentsev, I.D., & Makarov, D.I., 2001, Astrofizics, 44, 5

Karachentsev,I.D., Makarov, D.I., 1996, AJ, 111, 794

Kniazev, A.Y., Zijlstra, A.A., Grebel, E.K., et al. 2008, MNRAS, 388, 1667

Kobulnicky, H.A., Nordsieck, K.H., Burgh, E.B., et al., eds, Instrument Design and Performance for Optical/Infrared Ground-based Telescopes Vol. 4841 of Society of Photo-Optical Instrumentation Engineers (SPIE) Conference Series, Prime focus imaging spectrograph for the Southern African large telescope: operational modes. p. 1634

Makarov, D.I., Makarova, L.N., Sharina, M.E., et al. 2012, MNRAS, 425, 709

O'Donoghue, D., Buckley, D.A.H., Balona, L.A., et al., 2006, MNRAS, 372, 151

Oosterloo, T., Da Costa, G.S., & Staveley-Smith, L., 1996, AJ, 112, 1969

Peirani, S., & de Freitas Pacheco,J.A. 2008, A&A, 488, 845

Rizzi, L., Tully, R.B., Makarov, D., et al., 2007, ApJ, 661, 815

Sirianni, M., Jee, M. J., Bentez, N., et al., 2005, PASP, 117, 1049

Shaya, E.J., Peebles, P.J.E., & Tully, R.B., 1995, ApJ, 454, 15

Teerikorpi, P., Chernin, A.D., & Baryshev, Y.V., 2005, A&A, 440, 791

Tikhonov, A.V., & Klypin, A., 2009, MNRAS, 395, 1915

Tully, R.B., Rizzi, L., Shaya, E.J., et al., 2009, AJ, 138, 332 (=EDD)

Tully, R.B., Shaya, E.J., Karachentsev, I.D., et al., 2008, ApJ, 676, 184

van de Weygaert, R., & Schaap, W. 2007, in Data Analysis in Cosmology, ed. Martinez, V., et al. (Berlin: Springer)

Table 1   The Hubble flow for the nearby field galaxies

| Galaxy	SGL °	SGB °	$D_{MW}\pm$ Mpc	D_{LG} Mpc	$V_h\pm$ km s^{-1}	V_{LG} km s^{-1}	Θ_1	MD	V_{pec} km s^{-1}	T	SB $m/\square''$	M_B mag	lg[$sSFR$] yr^{-1}	lg M_{HI}/M^*
(1)	(2)	(3)	(4)	(5)	(6)	(7)	(8)	(9)	(10)	(11)	(12)	(13)	(14)	(15)
WLM	277.81	8.09	0.97 .02	0.82	-122 2	-16	0.0	M31	1	9	24.8	-14.1	- 9.93	0.14
ESO349-31	260.18	0.40	3.21 .16	3.10	221 6	230	0.0	N253	13	10	24.8	-11.9	-10.14	0.01
NGC0055	256.25	-2.36	2.13 .10	2.10	129 2	111	0.1	N300	-12	8	24.6	-18.4	- 9.70	-0.04
NGC0300	259.81	-9.50	2.15 .10	2.11	146 2	116	0.1	N55	-8	7	24.4	-17.9	- 9.97	-0.08
NGC0404	331.85	6.25	3.05 .15	2.63	-48 9	195	-0.8	Maffei2	20	-1	22.4	-16.5	-11.49	-1.35
KKs3	222.81	-21.34	2.12 .07	2.44	316 7	112	-1.4	M31	-45	-3	25.4	-11.8	-13.64	-2.34
HIZSS003	33.26	-78.42	1.67 .17	1.79	288 3	108	-1.1	M31	17	10	23.4	-12.8	-11.53	-0.22
NGC2403	30.80	-8.31	3.18 .16	3.15	133 1	270	0.2	DDO44	48	6	24.2	-19.2	- 9.95	-0.60
UGC04879	47.61	-15.01	1.36 .06	1.34	-25 4	33	-0.7	M31	-9	9	24.9	-11.9	-10.27	-1.00
LeoA	69.91	-25.80	0.80 .04	0.96	24 1	-40	-0.1	MW	-39	10	25.3	-11.7	-10.15	0.11
SexB	95.46	-39.62	1.43 .07	1.69	300 1	110	-0.8	MW	29	10	24.3	-14.0	-10.20	-0.12
NGC3109	137.96	-45.10	1.32 .06	1.68	403 2	110	0.2	Antlia	31	8	25.0	-15.7	- 9.95	0.20
SexA	109.01	-40.66	1.43 .07	1.74	324 2	94	-0.8	MW	8	10	24.2	-14.0	- 9.49	0.33
LeoP	84.87	-28.90	1.90 .05	2.14	262 2	135	-1.3	MW	8	10	24.4	- 9.3	-10.10	-0.17
NGC3741	67.96	-2.08	3.22 .16	3.34	229 2	263	-0.7	M81	25	9	23.8	-13.2	- 9.69	0.50
DDO99	74.93	-2.12	2.64 .14	2.74	251 2	257	-0.8	N4214	72	10	25.3	-13.5	- 9.71	0.32
IC3104	195.83	-17.06	2.27 .19	2.61	429 4	170	-1.2	N5128	-3	9	24.2	-14.8	-10.75	-1.48
DDO125	72.85	5.93	2.74 .14	2.81	206 2	251	-0.8	N4214	60	9	24.4	-14.3	-10.37	-0.62
GR8	102.98	4.67	2.13 .11	2.39	217 2	139	-1.4	MW	-13	10	24.4	-12.0	- 9.45	0.08
UGC08508	63.09	17.91	2.69 .14	2.67	56 2	181	-0.8	M81	3	10	24.3	-13.1	-10.20	-0.25
DDO181	78.09	18.58	3.01 .15	3.08	214 2	284	-1.1	N4736	68	10	24.7	-13.2	- 9.78	-0.20
DDO183	81.14	20.47	3.22 .16	3.38	188 2	254	-1.0	N4736	13	10	24.8	-13.2	-10.06	-0.21
KKH86	116.34	15.47	2.59 .13	2.89	287 1	209	-1.4	N5128	10	10	25.1	-10.3	-10.69	-0.60
UGC08833	83.54	21.09	3.08 .15	3.24	221 2	280	-1.1	N4736	51	10	24.2	-12.2	-10.26	-0.37
KK230	84.56	23.55	2.14 .10	2.26	63 2	127	-1.3	M81	-12	10	25.5	- 9.2	- 9.96	0.17
DDO187	97.83	24.35	2.24 .12	2.43	160 2	180	-1.4	MW	24	10	24.1	-12.5	-10.04	0.04
DDO190	74.07	26.85	2.80 .14	2.84	150 2	263	-1.2	M81	69	9	23.6	-14.2	-10.17	-0.40
KKR25	56.09	40.37	1.86 .12	1.79	-79 8	128	-1.0	M31	37	-1	25.8	- 9.4	-11.82	-1.80
IC4662	199.19	8.61	2.44 .18	2.74	302 3	139	-1.3	N5128	-46	9	22.4	-15.5	-10.10	-0.49
SagdIr	221.27	55.51	1.04 .07	1.14	-79 1	21	-0.4	MW	1	10	24.8	-11.5	- 9.65	0.43
DDO210	252.08	50.24	0.98 .05	0.97	-140 2	11	-0.3	MW	11	10	24.6	-11.1	-10.64	-0.33
IC5152	234.23	11.53	1.97 .12	2.08	122 2	73	-1.3	N253	-48	9	23.8	-15.6	-10.27	-0.70
KK258	255.48	18.58	2.23 .11	2.34	92 5	150	-1.1	N253	3	-3	26.0	-10.5	-11.64	-1.41
Tucana	227.61	-0.92	0.88 .04	1.09	194 4	73	-0.2	MW	59	-1	26.5	- 9.2	-12.66	-1.17
UGCA438	258.88	9.28	2.18 .12	2.11	62 8	99	-0.4	N55	-25	10	24.1	-12.9	-10.24	-0.34
KKH98	332.35	23.17	2.52 .13	2.11	-132 2	156	-0.9	Maffei2	32	10	25.1	-10.8	- 9.90	-0.13
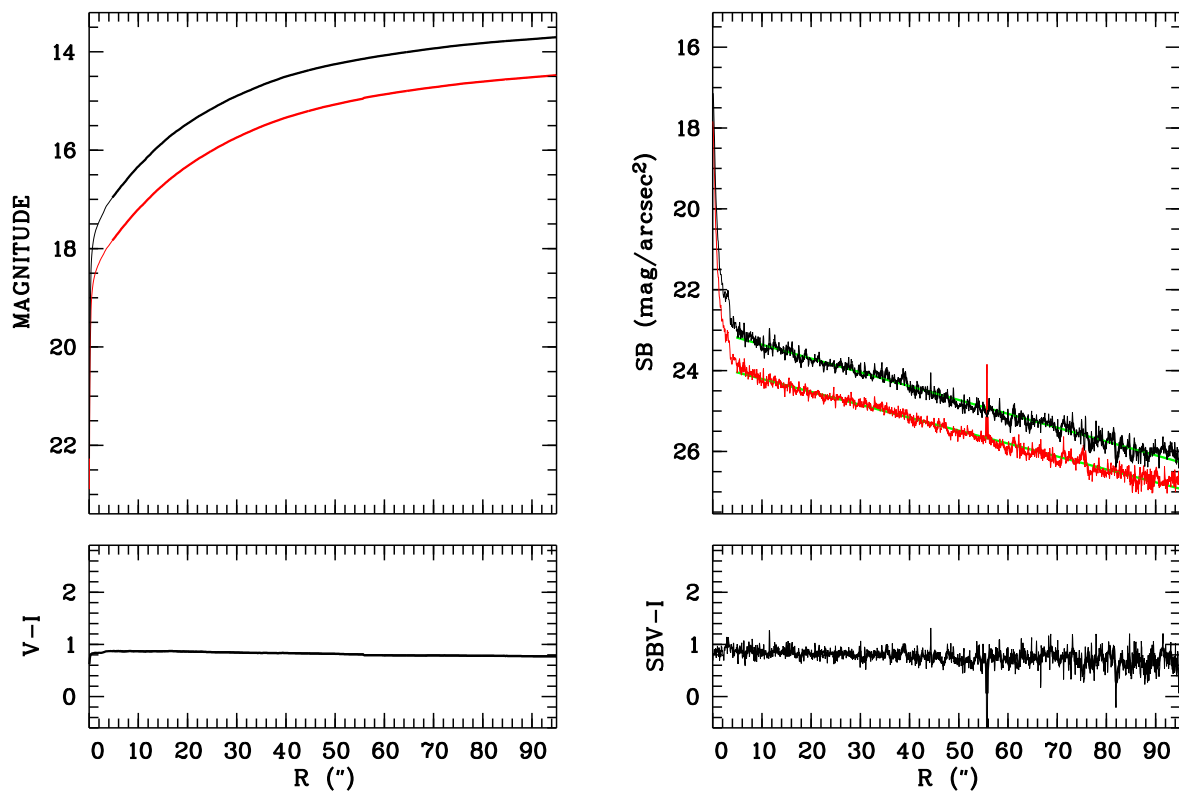
Fig. 1 Azimuthally averaged surface brightness profiles of KKS3 obtained with the HST/ACS. The I-band profile is going above the V-band one.
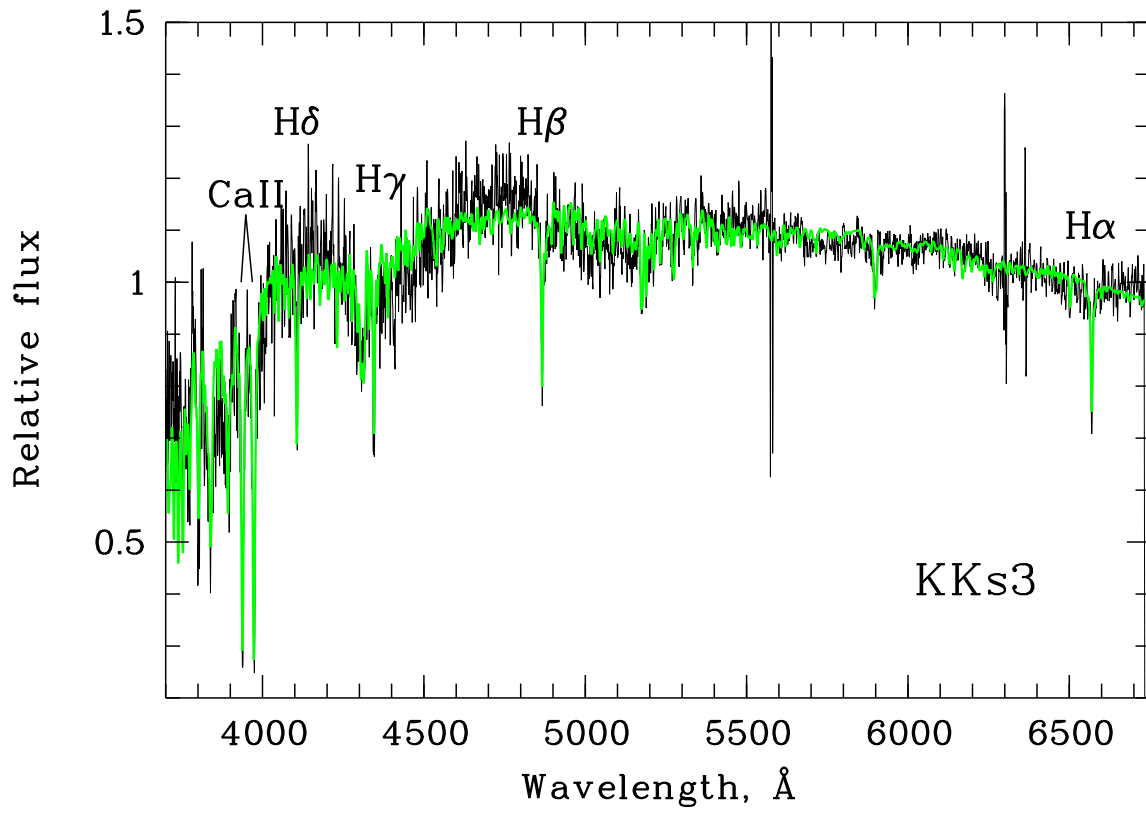
Fig. 2 One-dimensional scan of the spectrum of the globular cluster in KKs3 obtained with the SALT telescope. The fitting spectra was carried out with a composite model (green line) using the standard ULySS package
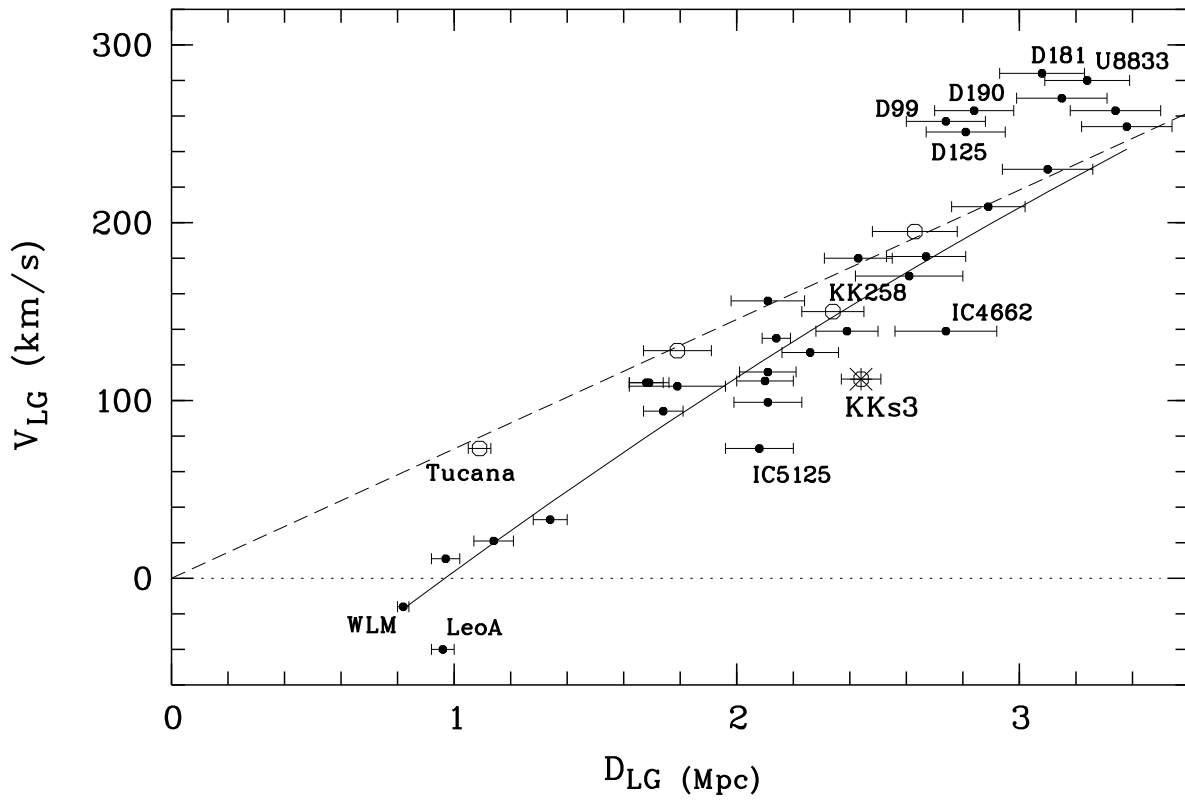
Fig. 3 The Hubble diagram for the nearby field galaxies. The galaxies of late ($T > 0$) and early types are denoted by the solid and open circles respectively (with distance errors). The dashed straight line denotes the undisturbed Hubble flow with a parameter of H_0 =73 km s^{-1} Mpc^{-1}. The solid line corresponds to the regression line $\langle V_{LG}|D_{LG}\rangle$ which crosses the zero-velocity line at $R_0 = 0.96$ Mpc.
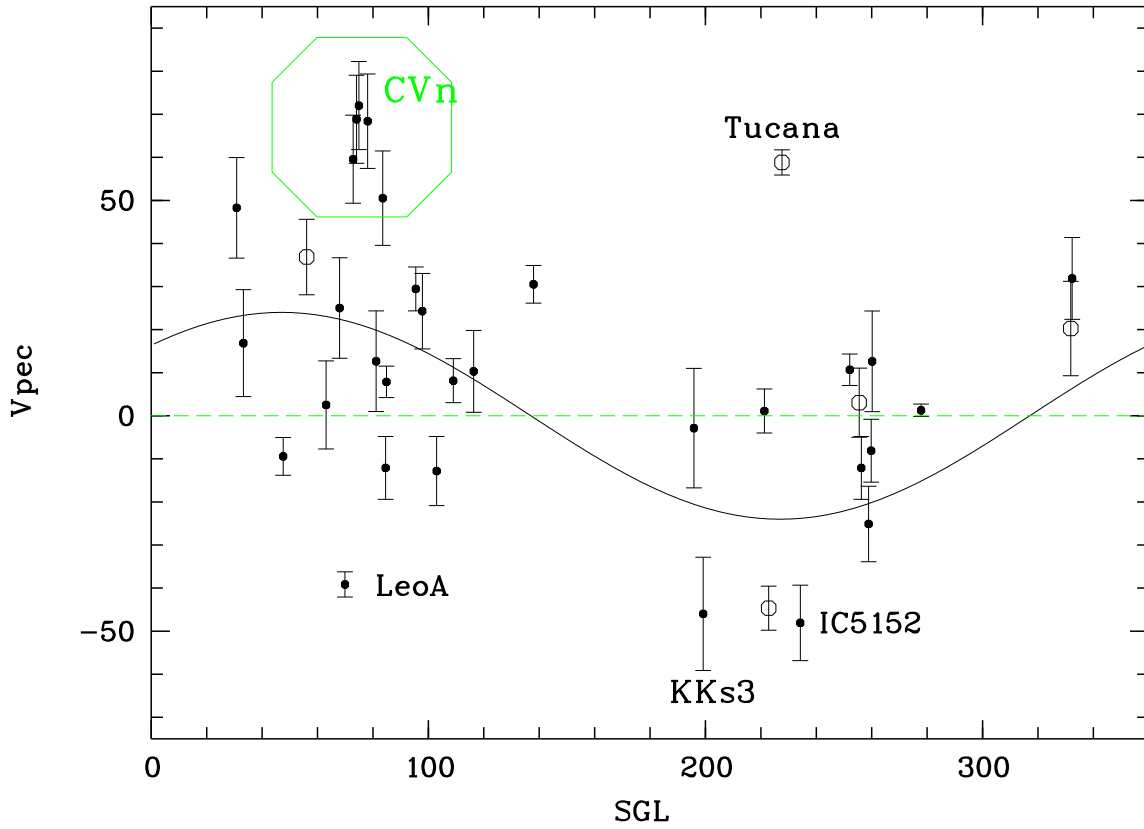
Fig. 4 Peculiar velocities of the nearby isolated galaxies in km s^{-1} as a function of their supergalactic longitude. The wavy line corresponds to the dipole component $V_d = 24\cos(\mathrm{SGL}-47)$. The notations for the late and early type galaxies are the same as in Fig. 3. The vertical intervals denote the errors in estimation of the galaxy velocities caused by the distance errors.
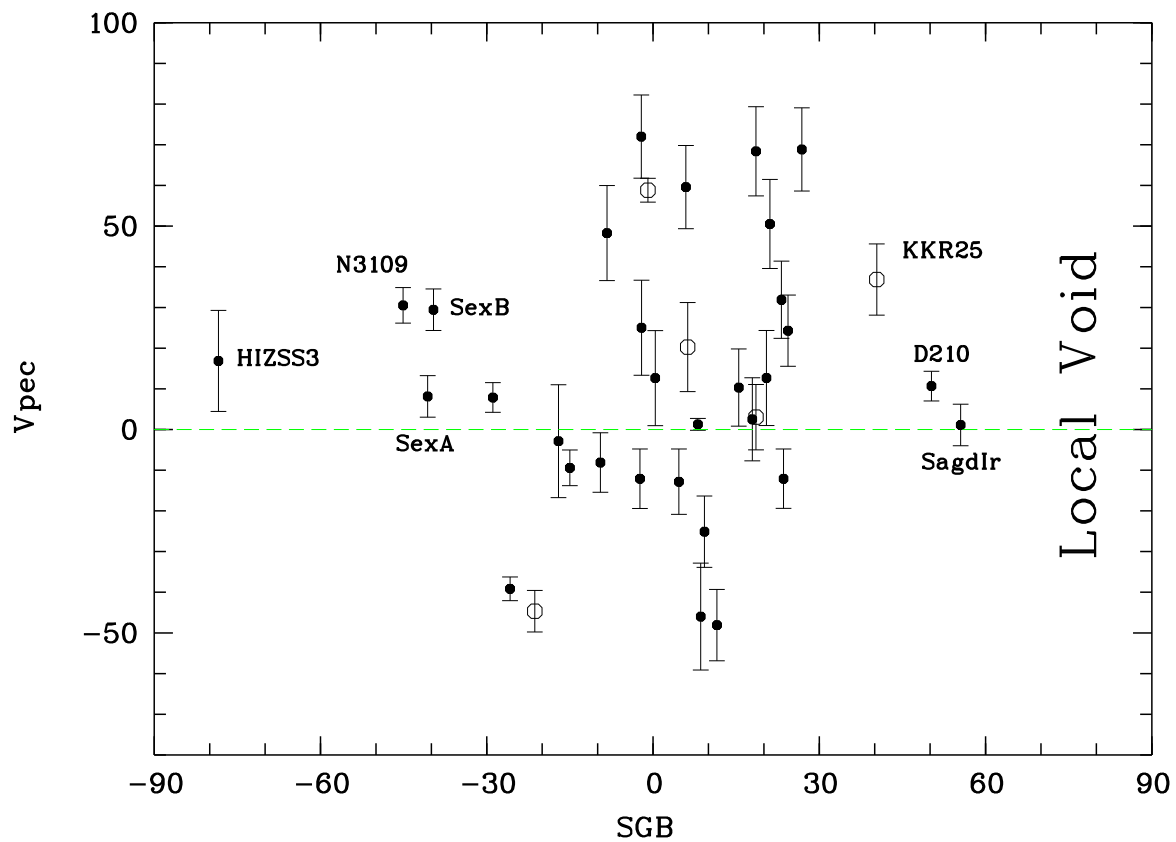
Fig. 5 Peculiar velocities of the nearby field galaxies in km s^{-1} versus their supergalactic latitude. The notations for the late and early type galaxies are the same as in Fig.3.
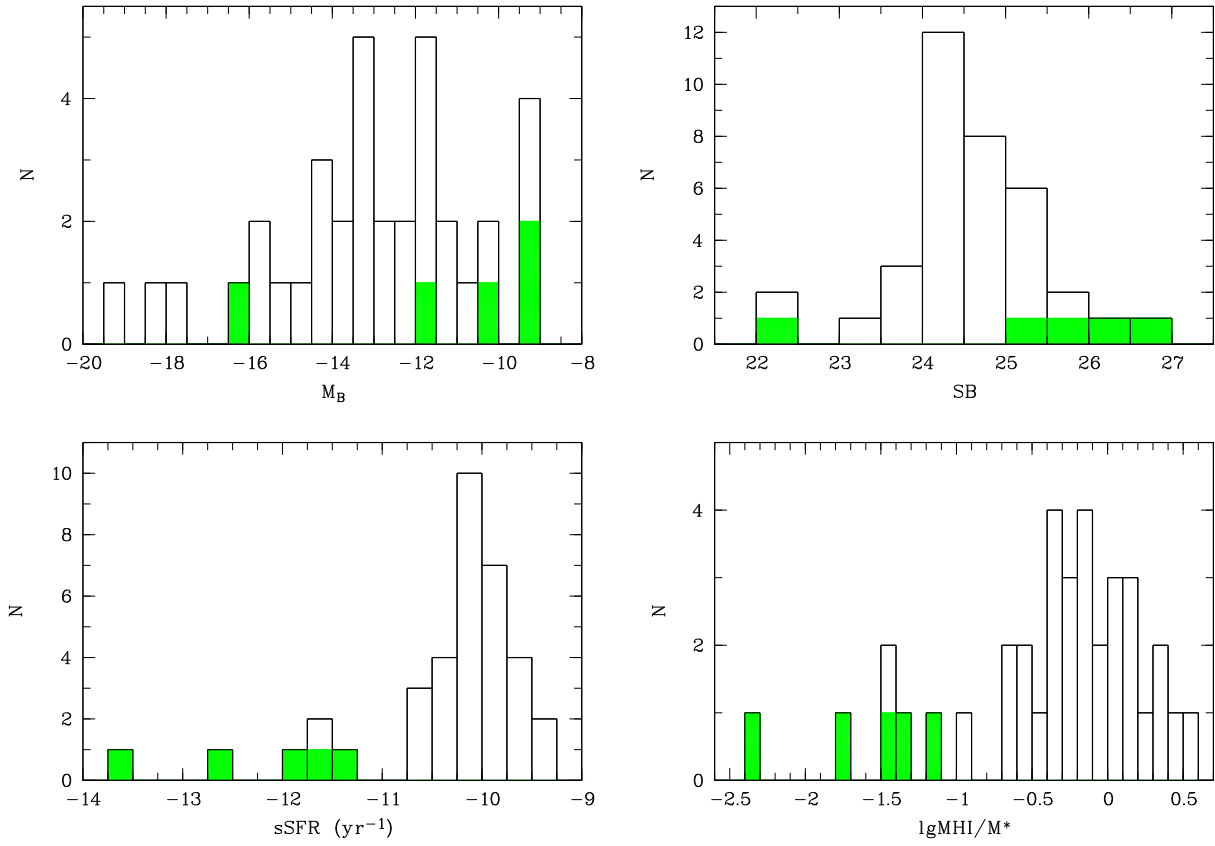
Fig. 6   A mosaic of histograms showing the distribution of 36 nearest field galaxies according to different parameters: the absolute B-magnitude, the average surface brightness within the Holmberg radius, the specific star formation rate, and the hydrogen mass-to- stellar mass ratio. The early type (S0, dSph, dTr) galaxies are highlighted in green.